Acta Metallurgica Sinica (English Letters) (2019) 32:1501–1510
https://doi.org/10.1007/s40195-019-00936-w

Effect of Co on Microstructure and Stress Rupture Properties of K4750 Alloy

Xiao-Xiao Li[1,2] · Mei-Qiong Ou[1] · Min Wang[1] · Xian-Chao Hao[1] · Ying-Che Ma[1] · Kui Liu[1]

Received: 24 April 2019 / Revised: 29 May 2019 / Published online: 13 September 2019

Abstract
The effects of substituting Co for Fe on the microstructure and stress rupture properties of K4750 alloy were studied. The microstructure of the alloy without Co (K4750 alloy) and the alloy containing Co (K4750-Co alloy) were analyzed. Substitution of Co for Fe inhibited the decomposition of *M*C carbide and the precipitation of η phase during long-term aging treatment. In K4750-Co alloy, the morphology of *M*C carbide at the grain boundary (GB) remained dispersed blocky shape and no η phase was observed after aging at 750 °C for 3000 h. However, in K4750 alloy, almost all the *M*C carbides at GBs broke down into granular $M_{23}C_6$ carbide and needle-like η phase. The addition of cobalt could delay the decomposition of *M*C carbides, which accordingly restricted the elemental supply for the formation of η phase. The stress rupture tests were conducted on two alloys at 750 °C/430 MPa. When Co is substituted for Fe in K4750 alloy, the stress rupture life increased from 164.10 to 264.67 h after standard heat treatment. This was mainly attributed to increased concentration of Al, Ti and Nb in γ' phase in K4750-Co alloy, which further enhanced the strengthening effect of γ' phase. After aging at 750 °C for 3000 h, substitution of Co for Fe can also cause the stress rupture life at 750 °C/430 MPa to increase from 48.72 to 208.18 h. The reason was mainly because *M*C carbide degradation and η phase precipitation in K4750 alloy, which promoted the initiation and propagation of micro-crack during stress rupture testing.

Keywords Nickel-based superalloy · Co addition · MC degradation · Stress rupture property

1 Introduction

Nickel-based superalloys are widely used for manufacturing critical components of aero engines due to their excellent mechanical properties and good resistance to oxidation and corrosion at elevated temperatures [1–3]. To meet the needs of high aero engine thrust–weight ratio and high-temperature performance, as one of the common methods, massive refractory elements such as Co, W and Mo are added into the alloys.

Previous works have reported that Co addition can affect the stacking-fault energy (SFE) and the features of precipitates like γ' and TCP phases in the alloys, which could generally induce changes in alloys' mechanical properties. For example, the substitution of Co for a part of Fe in In718 alloy inhibits the transition of γ'' phase to δ phase during the process of long-term aging at 650 °C, which is meaningful for the development of In718Plus alloy to meet the higher serving temperature requirements [4]. Wang et al. [5] stated that Co addition could retard the formation of TCP phase by accelerating the diffusion of elements in single-crystal superalloys. Yuan et al. found that the SFE of γ matrix is related to Co content in the Ni–Co-based superalloys. Lower SFE could enhance the ability to introduce more twin structures into the materials, which in turn improves the mechanical properties [6]. Zhuang et al. [7] believed that replacing Ni with Co in the Fe–Cr–Ni–Co superalloy (Refractoloy 26) increases the stability of *M*C carbides during aging treatment.

Recently, a new cast Ni-based superalloy K4750 has been developed for aircraft applications with operating

Available online at http://link.springer.com/journal/40195

✉ Mei-Qiong Ou
mqou@imr.ac.cn

✉ Ying-Che Ma
ycma@imr.ac.cn

[1] Institute of Metal Research, Chinese Academy of Sciences, Shenyang 110016, China

[2] School of Materials Science and Engineering, University of Science and Technology of China, Hefei 230026, China

temperature up to 750 °C, but the coarsening of γ' phase, the degradation of *M*C carbide and the precipitation of η phase during long-term aging cause the decrease in stress rupture properties [8–10].

As is known, Co is effective to increase the strength of γ phase and improve the creep properties of nickel-based superalloys, which can be attributed to the following aspects. Firstly, Co has an effect on the mismatch of γ/γ' phases, even though many researchers [1, 11] have suggested that the addition of Co does not significantly affect the lattice constants of γ and γ' phases and the mismatch between them. Nathal and Ebert [12] found that the γ/γ' mismatch increases with the increase in cobalt content in single-crystal superalloys. Secondly, Co affects the stability of *M*C carbides and γ' phases during long-term aging treatments. Some researchers have found that the addition of cobalt could reduce the coarsening rate of γ' phase and delay the decomposition of *M*C carbides [7, 12–14]. However, there is still no clear conclusion on the mechanism of the influence of Co on the microstructure stability of superalloys. Thirdly, Co improves the creep properties of superalloys by reducing the stacking-fault energy of γ matrix [15–17]. The stacking-fault energy significantly influences the creep process due to the climb and cross slip of the dislocations in γ matrix or the introduction of more twin structures in superalloy [6]. Finally, Co inhibits the precipitation of topologically close-packed phases (TCP) in superalloy. One explanation was that Co can promote the diffusion of elements and prohibit the formation of elemental segregation, which in turn reduce the tendency to form TCP phases [5]. Another explanation was that the addition of Co can also increase the lattice constant of γ and the mismatch of γ/σ surface, which reduces the nucleation rate of σ phase [18]. Therefore, the μ phase, where σ phase was the growth site, would also be suppressed.

Based on the above analysis, Co is beneficial to the mechanical properties of the superalloy, but the strengthening mechanism varies with the alloy system. Until now, the influence of Co on the microstructure stability of K4750 alloy is still unclear. Therefore, the effects of Co on the microstructure and stress rupture properties of K4750 alloy were studies in this work, and after stress rupture testing, the relationship between the microstructure evolution and the stress rupture properties of K4750 and K4750-Co alloys was explained.

2 Experimental

The cast ingots of the alloy without Co (K4750 alloy) and the alloy containing Co (K4750-Co alloy) were melted in a vacuum induction melting (VIM) and then were cast into the bars with a diameter of 15 mm. The chemical compositions of two alloys were determined using the inductively coupled plasma atomic emission spectrometer (ICP-AES), as shown in Table 1. In this study, all bars of K4750 and K4750-Co alloys were firstly subjected to a standard heat treatment (SHT), which includes the hot isostatic pressing at 1165 °C/135 MPa for 4 h followed by furnace cooling, the solution annealing at 1120 °C for 4 h followed by air cooling and the aging treatment at 800 °C for 20 h followed by air cooling. After the standard heat treatment, three bars of each alloy were carried out long-term aging treatments at 750 °C for 3000 h (SHT + 750 °C/3000 h). Two bars were taken from two alloys in SHT and SHT + 750 °C/3000 h condition for processing into stress rupture samples with a gauge diameter of 5 mm and a gauge length of 25 mm, and then, the samples were tested at 750 °C and 430 MPa. The average value of two stress rupture samples was used to determine the stress rupture life and elongation.

The microstructure of the samples in SHT and SHT + 750 °C/3000 h condition was studied by an Axio Observer ZIm optical microscope (OM), an INSPECT F50 field emission scanning electron microscope (SEM), a JEOL JXA-8230 electronic probe (EPMA), a Tecnai 30 transmission electron microscope (TEM) equipped with energy dispersive spectroscopy (EDS) and a LEAP5000XR three-dimensional atom probe tomography (3D-APT). The fracture surface and the longitudinal microstructure of stress ruptured samples were studies by SEM.

The OM, SEM and EPMA samples were etched by a solution with 20 g $CuSO_4$, 100 ml HCl, 5 ml H_2SO_4 and 100 ml H_2O. In order to investigate the morphology and distribution of γ' phase, a kind of deep etching method was employed using a solution with 13 ml H_3PO_4, 42 ml H_2SO_4 and 45 ml HNO_3. TEM samples were mechanically thinned down to about 60 μm and were electro-polished in a chemical solution of 10% perchloric acid in ethanol solution at − 15 °C and 20 V. The 3D-APT samples were cut into 0.5 mm × 30 mm cylindrical type from the K4750 and K4750-Co alloys after the standard heat treatment, and then, samples were electro-polished into needles with an approximate tip diameter of 100 nm. The electro-polishing was conducted in two steps: a coarse polish

Table 1 Chemical compositions of K4750 and K4750-Co alloys (wt%)

Alloy	C	Cr	W + Mo	Ti + Al + Nb	B	Ni	Fe	Co
K4750	0.12	20.18	4.75	5.50	0.0093	Bal.	4.33	0
K4750-Co	0.12	19.36	4.53	5.60	0.0070	Bal.	0	3.99

using the 10% perchloric acid in acetic acid solution at about 20 V and a fine polish using the 4% perchloric acid in butoxyethanol solution at about 10 V.

3 Results and Discussion

3.1 Microstructure Evolution During Standard Heat Treatment

After standard heat treatment, the typical microstructures of K4750 and K4750-Co alloys contain γ matrix, γ' phase, *M*C and $M_{23}C_6$ carbides are shown in Fig. 1. The morphology of *M*C carbide is blocky, and most of them distribute in γ matrix and a few distribute at the grain boundaries (GBs). $M_{23}C_6$ carbides are in a fine granular shape and discretely distribute at GBs. γ' phase is fine spherical and homogeneously distributes in γ matrix.

3.2 Microstructure Evolution During Long-Term Aging

Figure 2 shows the microstructure of K4750 and K4750-Co alloys after long-term aging at 750 °C for 3000 h. Figure 2a displays the decomposition of *M*C carbides in K4750 alloy and the needle-like phases around *M*C carbides and in the vicinity of GBs. In contrast, *M*C carbides in K4750-Co alloy remained blocky and there was no evidence of the generation of needle-like phase. The $M_{23}C_6$ carbides of two alloys were still fine granular and discretely distributed on GBs. When it comes to the γ' phases, it kept its spherical morphology and the uniform distribution, but the size obviously increased after long-term aging. In order to quantitatively determine the coarsening of γ' phase, the average radii of γ' phases for all specimens were measured by the Image-Pro Plus software. After standard heat treatment and the long-term aging at 750 °C for 3000 h, the average radius of γ' phase in K4750 alloy was about 61.71 nm and 103.69 nm, while in K4750-Co alloy it was about 57.85 nm and 98.75 nm. In other words, the size, distribution and morphology of γ' phases of these two alloys were basically identical regardless of heat treatment condition. The reasons for the difference in the degradation of *M*C carbide and the precipitation of needle-like phase between two alloys during long-term aging treatment would be discussed below.

Figure 3 shows the EPMA analysis of degenerated *M*C carbide in K4750 alloy after long-term aging at 750 °C for 3000 h. The SEM and EPMA images of K4750 alloy after long-term aging (Figs. 2b, 3a) indicated that the *M*C decomposition resulted in the formation of decomposition zone. To be specific, degraded *M*C carbides were surrounded by a kind of discrete particles and the needle-like phases. As could be seen from the EPMA analysis results in Fig. 3, C, Ti and Nb were enriched in the center of the decomposition zone, which could be identified as the original *M*C carbides. The discrete particles at the edge of degraded *M*C were identified by EPMA as Cr-rich $M_{23}C_6$ carbides, which can be verified by the TEM analysis in Fig. 4. The needle-like phase

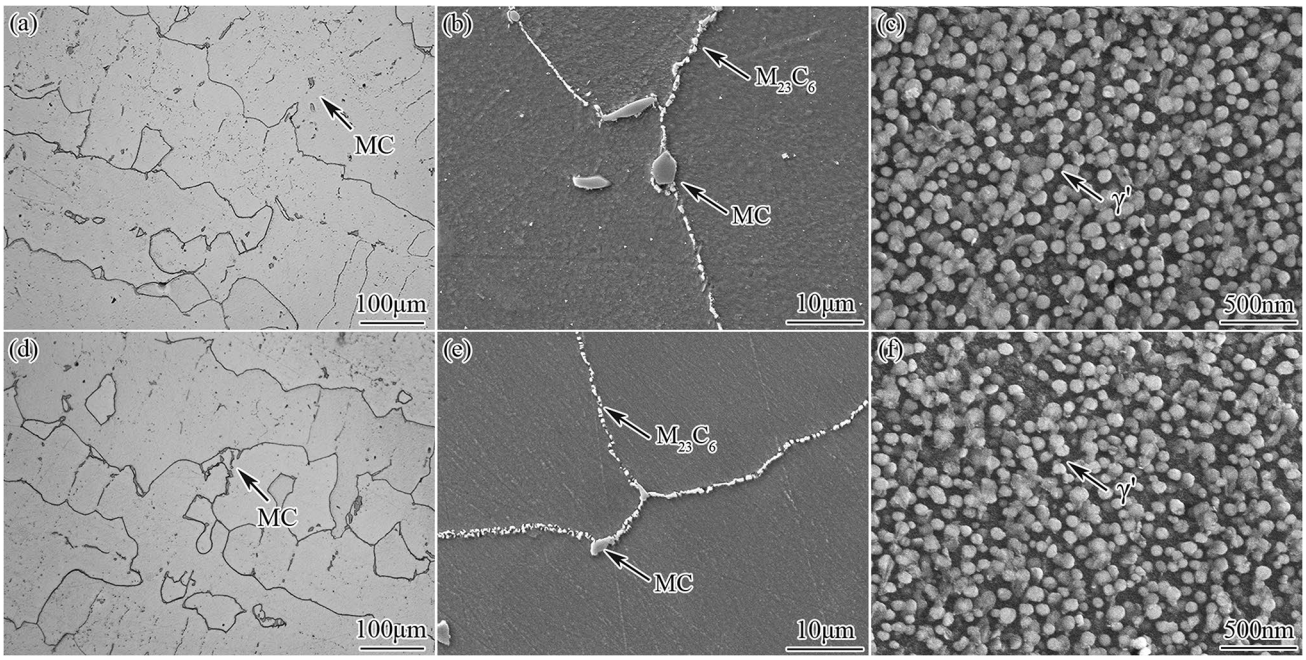

Fig. 1 Microstructures of K4750 alloy **a**–**c**, K4750-Co alloy **d**–**f** after standard heat treatment: **a**, **d** *M*C carbide; **b**, **e** $M_{23}C_6$ carbide; **c**, **f** γ' phase

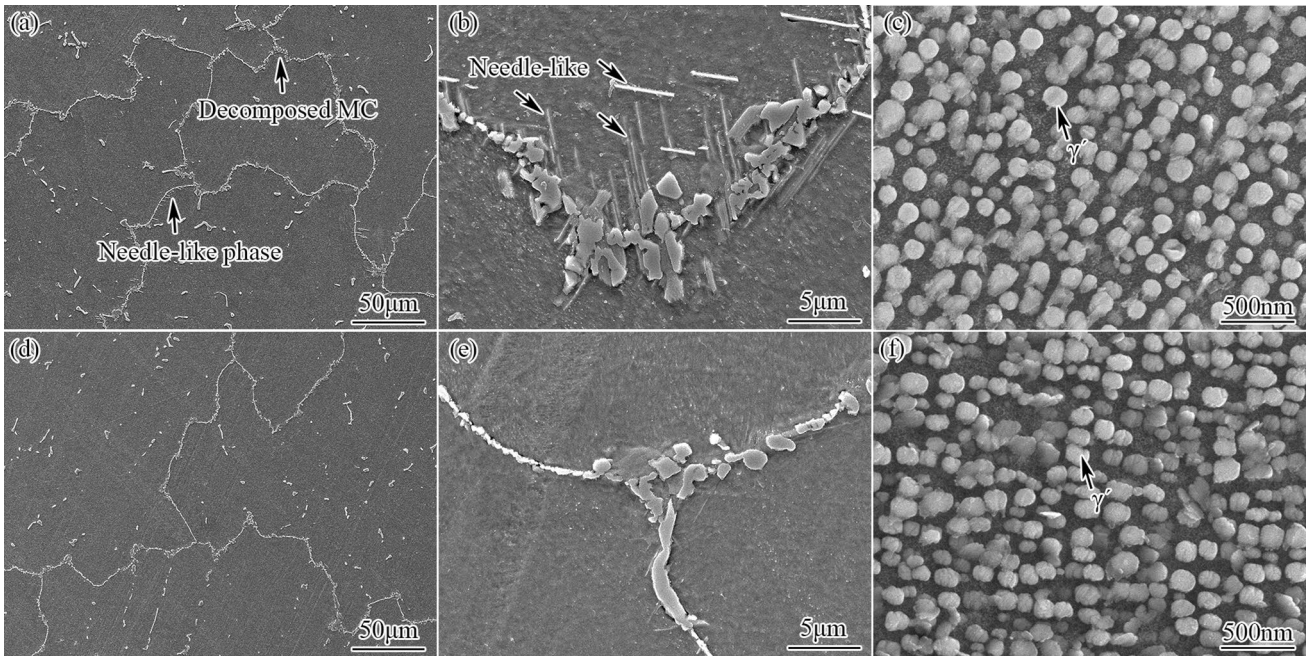

Fig. 2 Microstructures of K4750 alloy **a**–**c**, K4750-Co alloy **d**–**f** after long-term aging at 750 °C for 3000 h: **a**, **d** decomposed *M*C; **b**, **e** needle-like phase; **c**, **f** γ' phase

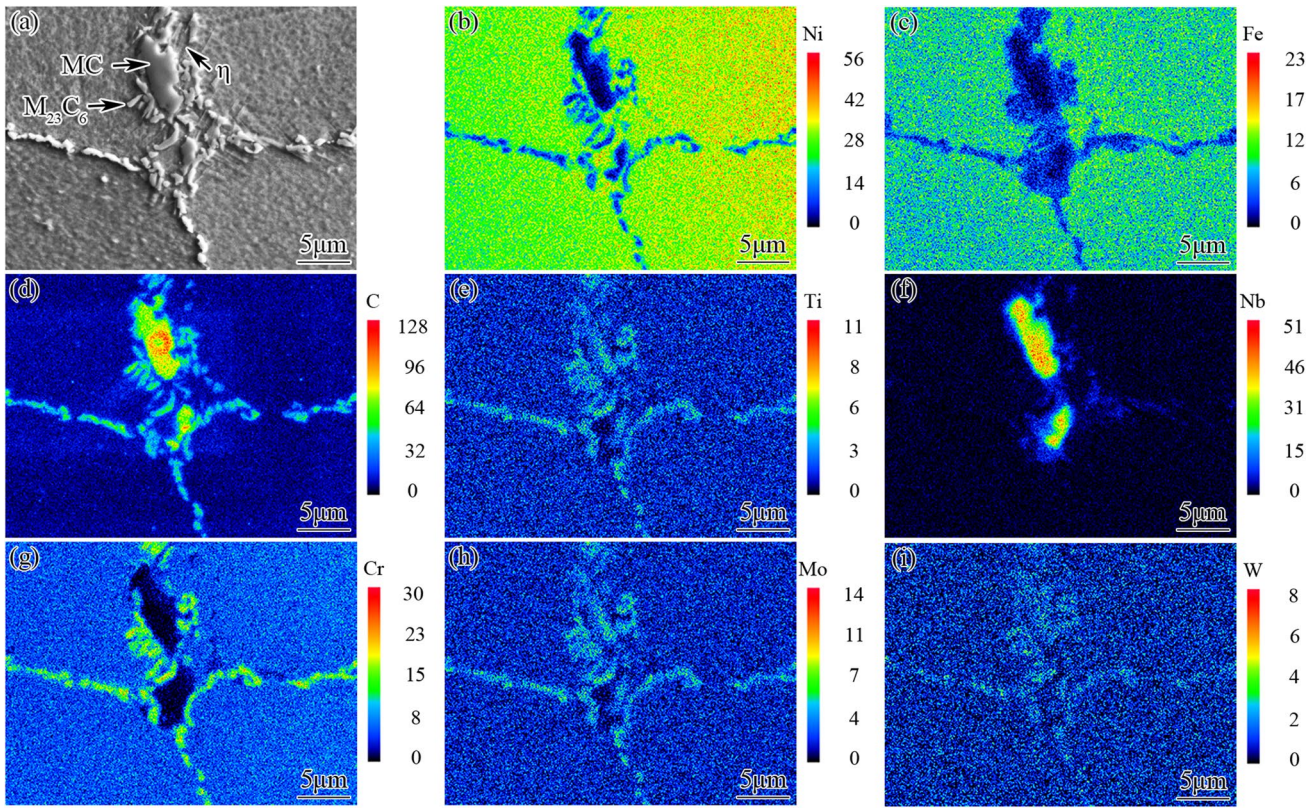

Fig. 3 EPMA analysis of degenerated MC carbide in K4750 alloy after long-term aging at 750 °C for 3000 h: **a** secondary electron image; **b** Ni; **c** Fe; **d** C; **e** Ti; **f** Nb; **g** Cr; **h** Mo; **i** W

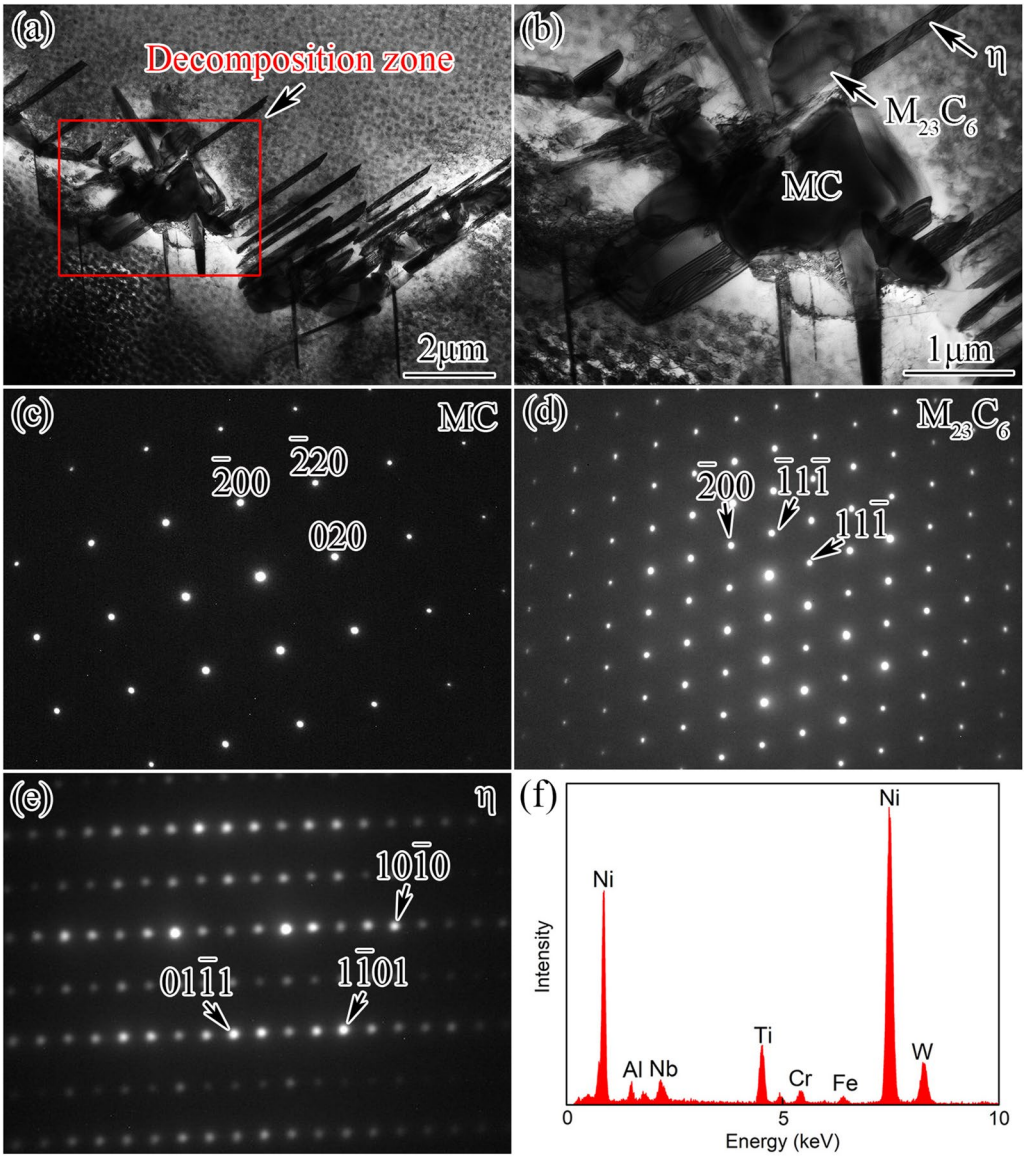

Fig. 4 TEM analysis of K4750 alloy after long-term aging at 750 °C for 3000 h: **a**, **b** decomposition zone images; selected area diffraction pattern of **c** *M*C, **d** $M_{23}C_6$ and **e** η phase; **f** EDS spectrum of η phase

was identified to be η phase by means of selected area diffraction pattern and EDS spectra. The decomposition of *M*C carbides resulted in the formation of granular $M_{23}C_6$ and needle-like η phases, and this reaction can be written as:

$$MC + \gamma \rightarrow M_{23}C_6 + \eta. \quad (1)$$

Figure 5 shows the distribution of carbon element in degraded *M*C carbide from the center to the edge by EPMA. A significant reduction in carbon content suggested that the carbon element of original *M*C carbides diffused from the center to the edge during long-term aging treatment. Then, carbon at the edge of *M*C carbides combined with the chromium in γ matrix to form Cr-rich $M_{23}C_6$ phase. Due to the high concentration of Ti in decomposition zone and its low diffusivities, the composition requirement for the formation of η phase was easily satisfied [19]. Finally, granular $M_{23}C_6$ and needle-like η phases were precipitated near the degenerated *M*C carbide. The degradation of *M*C carbide was accompanied by the formation of $M_{23}C_6$ and η phases by combining the Cr and Ti, which can be described in Fig. 6. This conclusion is consistent with other studies [19–22].

Figure 7 shows the EPMA analysis of *M*C carbide in K4750-Co alloy after long-term aging at 750 °C for 3000 h. Although *M*C carbides were still blocky in shape, there were some small particles at the edges of *M*C carbides that were hard to be distinguished, as indicated by the arrows in Fig. 7a. The TEM image in Fig. 8 also shows that there is smaller phase next to blocky *M*C carbide. Chromium enriched in

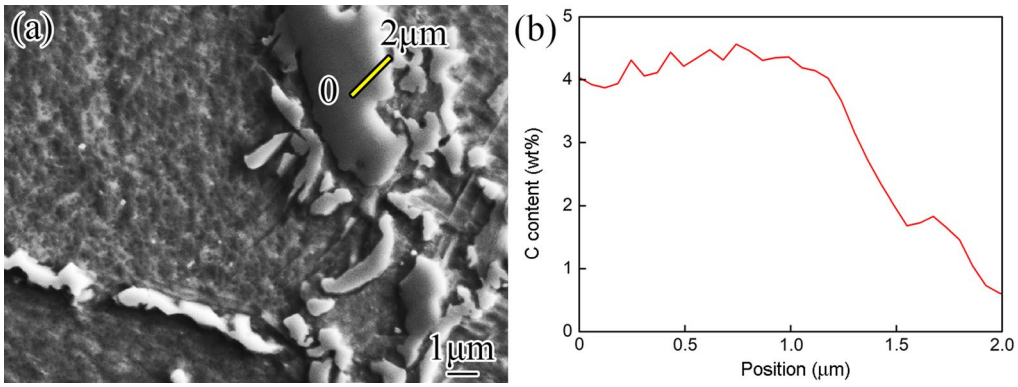

Fig. 5 Distribution of C in *M*C carbide of K4750 alloy after long-term aging at 750 °C for 3000 h

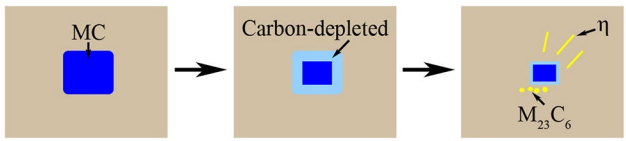

Fig. 6 Schematic diagrams of *M*C carbide degradation in K4750 alloy during long-term aging

small granular phases could be preliminarily determined by the Cr element distribution map. It was further identified as Cr-rich $M_{23}C_6$ phase by selective electron diffraction and energy spectrum analysis, as shown in Fig. 8c and d. The results show that the degree of *M*C carbide degeneration in K4750-Co alloy was slighter than that in K4750 alloy during long-term aging treatment. The addition of cobalt inhibited

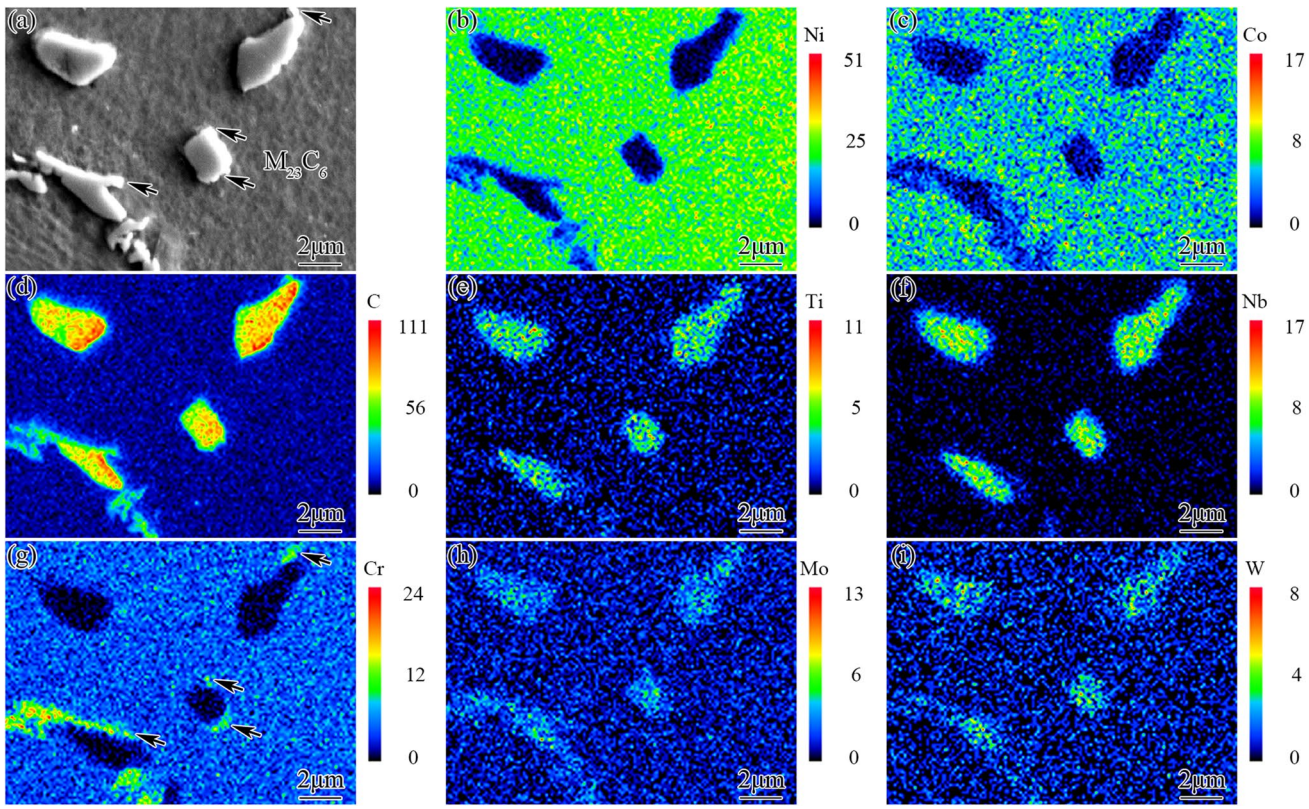

Fig. 7 EPMA analysis of *M*C carbides in K4750-Co alloy after long-term aging at 750 °C for 3000 h: **a** secondary electron image; **b** Ni; **c** Fe; **d** C; **e** Ti; **f** Nb; **g** Cr; **h** Mo; **i** W

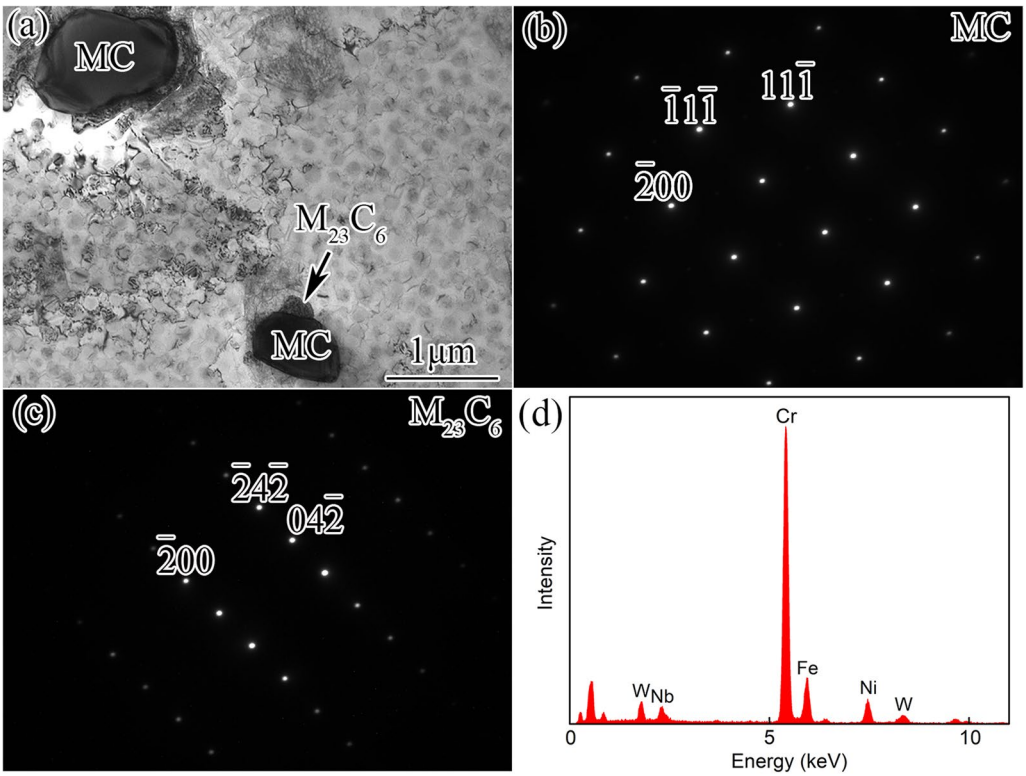

Fig. 8 **a** TEM morphology of K4750-Co alloy after long-term aging at 750 °C for 3000 h, selected area diffraction pattern of **b** *M*C, **c** $M_{23}C_6$, **d** EDS spectrum of $M_{23}C_6$

*M*C carbides degradation. Besides, no needle-like η phase was observed in K4750-Co alloy after long-term aging. The formation of η phase was closely related to the atomic ratio of (Ti + Ta + Nb + Hf)/Al in superalloy [23]. With the increase in the decomposition degree of primary *M*C carbides, the atomic ratio of (Ti + Ta + Nb + Hf)/Al near the interface of *M*C increased, which could promote the generation of η phase [24]. The decomposition of *M*C carbides in K4750-Co alloy was restrained, which accordingly restricted the elemental supply for the formation of η phase.

3.3 Stress Rupture Properties of Two Alloys

After SHT or SHT + 750 °C/3000 h, K4750 and K4750-Co alloys were carried out stress rupture tests at 750 °C and 430 MPa. The stress rupture life and elongation of these two alloys are listed in Table 2.

In the condition of SHT, the stress rupture lives of K4750 and K4750-Co specimens are 164.10 h and 264.67 h, and the elongations are 10.4% and 9.7%, respectively. After being aged at 750 °C for 3000 h, the stress rupture life increased from 48.72 to 208.18 h and the elongation decreased from 16.0 to 7.4% when the Fe in K4750 alloy was replaced by Co.

The above results indicate that K4750-Co alloy possesses a longer stress rupture life than K4750 alloy in SHT and SHT + 750 °C/3000 h conditions. However, K4750 alloy without Co displays better ductility after long-term aging. After Fe was replaced by Co in K4750 alloy, the change of stress rupture lives and elongation may be related to microstructure evolution. The following sections would focus on the effect of microstructure on the stress rupture properties.

Table 2 Stress rupture properties of K4750 and K4750-Co specimens in SHT and SHT + 750 °C/3000 h conditions

Alloy	Heat treatment	Life (h)	Elongation (%)	Heat treatment	Life (h)	Elongation (%)
K4750	SHT	164.10	10.4	SHT + 750 °C/3000 h	48.72	16.0
K4750-Co		264.67	9.7		208.18	7.4

3.4 Correlation Between Microstructure and Stress Rupture Property

There was little difference in the morphology, size and distribution of precipitates between K4750 and K4750-Co alloys after standard heat treatment. However, the stress rupture life of K4750-Co alloy was about 100 h higher. In order to investigate the reasons behind the change of stress rupture life, the composition of γ' phase was studied. Figure 9 displays the concentration variation of Al, Ti and Nb at the γ/γ' phase surface of K4750 and K4750-Co alloys in the condition of standard heat treatment obtained by atomic probe analysis. The contents of Al and Ti in the γ' phase of K4750-Co alloy were higher than that of K4750 alloy. Al and Ti were the main forming elements of γ' phase in nickel-based superalloys, and the strengthening effect of γ' phase could be enhanced by the increase in Al and Ti content [25]. Maniar et al. [26, 27] found that the dissolution temperature of γ' phases increases with the increase in Ti and Al content, thus improving the high-temperature strength of the Ni20Cr base heat-resistant alloy. Besides, Nb was detected in γ' phase of K4750-Co alloy, but not in K4750 alloy. Nb atoms entering the γ' phase could significantly increase the lattice constant of γ' phase and thus improved the lattice mismatch between γ matrix and γ' phase, which could play a mismatch strengthening effect in nickel-based alloy [28, 29]. Substituting Co for Fe increased the concentration of Al, Ti and Nb in γ' phase and improved the strengthening effect of γ' phase, which resulted in a longer stress rupture life of K4750-Co alloy after standard heat treatment.

After long-term aging at 750 °C for 3000 h, the longitudinal microstructure near ruptured surface of K4750 and K4750-Co specimens was investigated, as shown in Fig. 10. Micro-cracks and micro-voids were found in K4750 and K4750-Co alloys at GBs. The degradation of *M*C carbides at GBs resulted in a decomposition zone with granular $M_{23}C_6$ and needle-like η phases in K4750 alloy after long-term aging. Micro-cracks are mostly formed in decomposition zone, and some micro-cracks were connected with each other to form long cracks (Fig. 10b). The production of micro-cracks could accelerate the fracture process of superalloys [30]. Therefore, *M*C degeneration in K4750 alloy resulted in a much larger cracking incidence than intact *M*C in K4750-Co alloy, which could significantly reduce stress rupture life. The reason why cracks can easily produce and expand in the decomposition zone was that the decomposition products of primary *M*C carbides provided higher interfacial energy [31]. Besides, there was needle-like η phase in K4750 alloy after long-term aging (Fig. 3). Needle-like η phases obviously impeded the gliding of dislocations, and the existence of dislocation pileup would induce the stress concentration at η phase/matrix interface, which was able to promote the nucleation of micro-cavities and micro-cracks [32, 33]. On the contrary, the blocky *M*C carbides remained intact and no η phase was observed in K4750-Co alloy after long-term aging. The blocky *M*C carbides at the GBs prevented the micro-void from further expanding into micro-crack, as shown in Fig. 10d. From this point of view, the K4750-Co alloy after long-term aging had a longer stress rupture life than K4750 alloy.

When Co was substituted for Fe, there was little difference in the stress rupture elongation between two alloys after standard heat treatment, but the stress rupture elongation decreased from 16.0 to 7.4% after long-term aging at 750 °C for 3000 h. Figure 11 shows the fracture surfaces and the longitudinal microstructures of stress rupture samples (K4750 and K4750 alloys after long-term aging). The fracture surfaces with dimples and micro-cracks of two alloys exhibited a mixed mode of transgranular and intergranular fracture. Among them, the dimples in K4750 alloy were more obvious, which indicated better plasticity. The SEM images of longitudinal sections showed that the micro-voids in the decomposition zone near the GBs of K4750 alloy were difficult to coalesce into micro-cracks, which were blocked by dispersed granular $M_{23}C_6$ carbides. However, the continuous $M_{23}C_6$ carbides in K4750-Co alloy were very hard to restrain the propagation of micro-cracks along GBs. During stress rupture tests, continuous $M_{23}C_6$

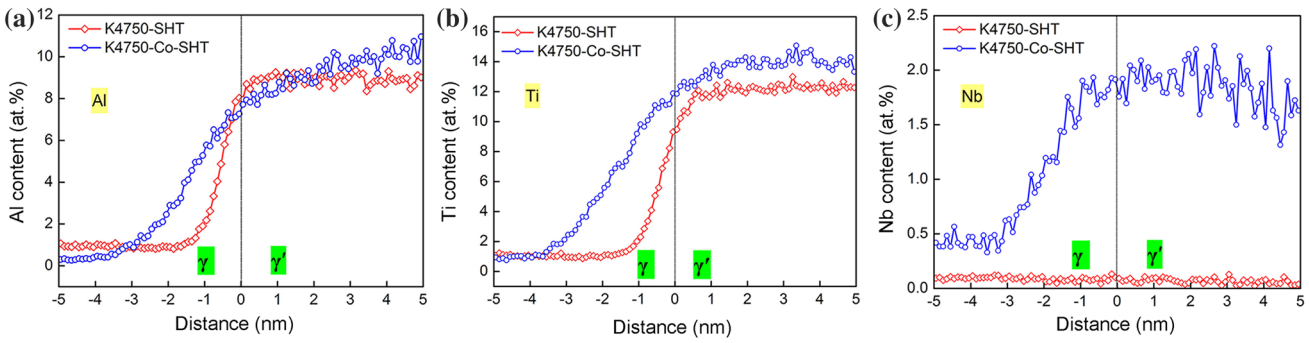

Fig. 9 Concentration variation of **a** Al, **b** Ti,**c** Nb at γ/γ' interface of K4750 and K4750-Co alloy after standard heat treatment

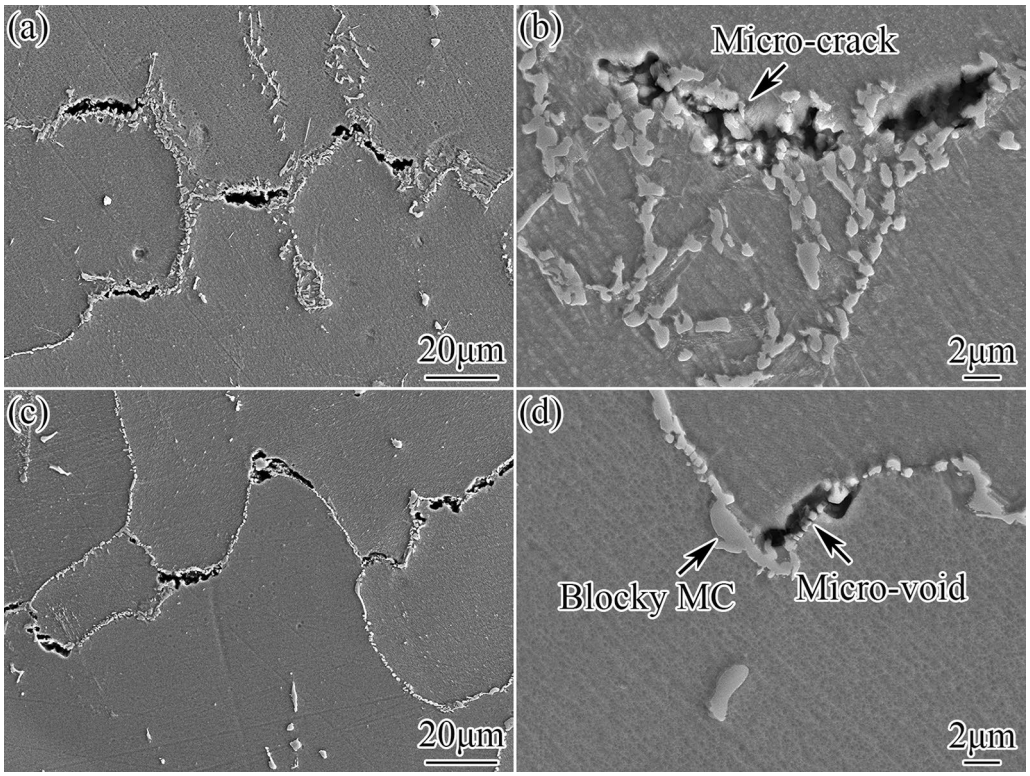

Fig. 10 Longitudinal microstructures of stress rupture specimens in long-term aging condition: **a**, **b** K4750 alloy; **c**, **d** K4750-Co alloy

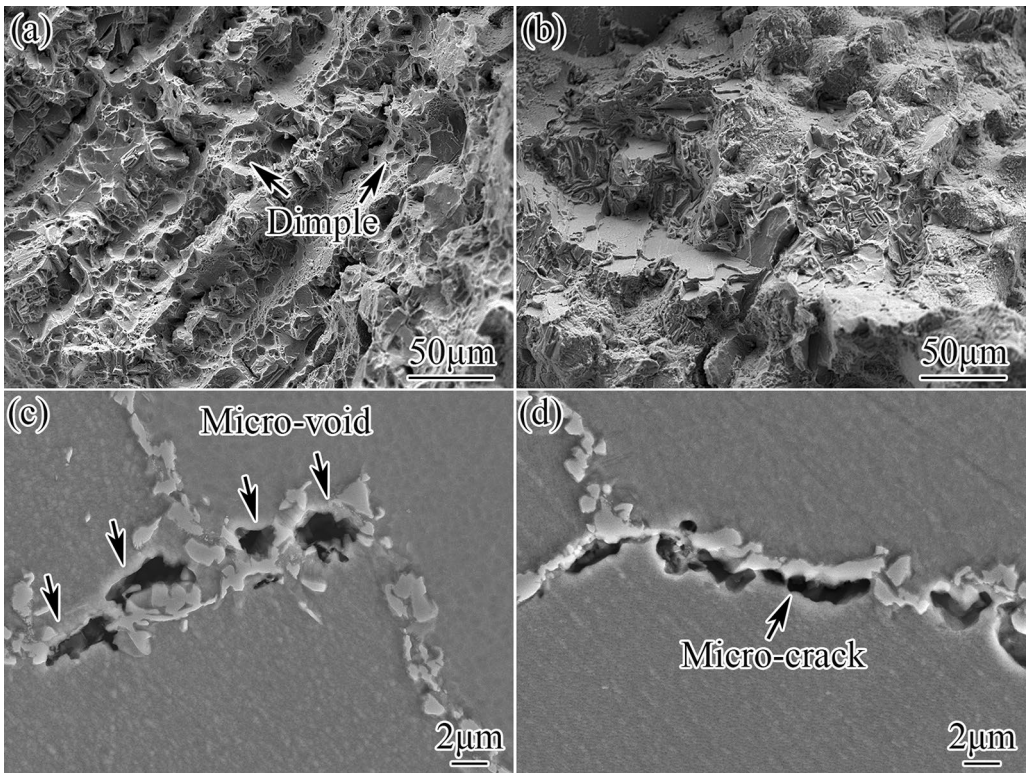

Fig. 11 Fracture surfaces and longitudinal microstructures of stress ruptured specimens in long-term aging condition: **a**, **c** K4750 alloy; **b**, **d** K4750-Co alloy

carbides resulted from long-term aging of K4750-Co alloy impeded the dislocation movement and produced stress rupture concentrations at GBs [34, 35], thus lowering the stress rupture plasticity. Conversely, granular $M_{23}C_6$ carbides in decomposition zone of K4750 alloy after long-term aging were benefit to release the GBs stress concentrations [36], and thus, the stress rupture plasticity increased. Therefore, the main reason for the increase in plasticity was the large amount of dispersed granular $M_{23}C_6$ phase produced by the decomposition of *M*C carbides in K4750 alloy after long-term aging.

4 Conclusions

(1) The effects of substituting Co for Fe on the microstructure and stress rupture properties of K4750 alloy were investigated. After long-term aging at 750 °C for 3000 h, *M*C carbide was decomposed obviously and needle-like η phase were formed in K4750 alloy. The *M*C decomposition reaction could be written as: $MC+\gamma \rightarrow M_{23}C_6+\eta$. Specifically, the decomposition of primary *M*C carbide resulted in a decomposition zone with granular $M_{23}C_6$ carbides and needle-like η phases. On the contrary, *M*C carbides remained blocky and no η phase was precipitated in K4750-Co alloy. The addition of cobalt could delay the decomposition of *MC* carbides in the long-term aging process and thus inhibited the formation of η phase.

(2) When Co was substituted for Fe in K4750 alloy, the stress rupture lives increased from 164.10 to 264.67 h after standard heat treatment. This was mainly attributed to the increase in concentration of Al, Ti and Nb in the γ' phase of K4750-Co alloy, which further enhanced the strengthening effect of γ' phase.

(3) After long-term aging at 750 °C for 3000 h, the stress rupture life of K4750 and K4750-Co alloys was 48.72 h and 208.18 h, respectively. However, the stress rupture elongation of K4750-Co alloy was lower than that of K4750 alloy. The tendency of crack formation at the decomposed *M*C carbide in K4750 alloy is greater than the intact MC carbide in K4750-Co alloy, which could significantly reduce stress rupture life of K4750 alloy. The formation of needle-like η phase at the edge of the degenerated *M*C would facilitate the nucleation and propagation of micro-crack. The dispersed granular $M_{23}C_6$ phases produced by *M*C degradation could not only release the stress concentration but also hinder the crack propagation and thus improved the stress rupture plasticity of K4750 alloy.

References

[1] R.C. Reed, *The Superalloys: Fundamentals and Applications* (Cambridge University Press, New York, 2006)
[2] C.T. Sims, W.C. Hagel, *The Superalloys-Vital High Temperature Gas Turbine Materials for Aerospace and Industrial Power* (Wiley, New York, 1972)
[3] T.M. Pollock, S. Tin, J. Propuls. Power **22**, 361 (2006)
[4] X. Xin, W.H. Zhang, L.X. Yu, F. Liu, Mater. Sci. Forum **816**, 613 (2015)
[5] W.Z. Wang, T. Jin, J.L. Liu, X.F. Sun, H.R. Guan, Z.Q. Hu, Mater. Sci. Eng. A **479**, 148 (2008)
[6] Y. Yuan, Y.F. Gu, C.Y. Cui, T. Osada, Z.H. Zhong, T. Tetsui, T. Yokokawa, H. Harada, MRS Bull. **26**, 2833 (2011)
[7] L.Z. Zhuang, G.L. Chen, J.L. Xu, Mater. Mech. Eng. **2**, 11 (1987)
[8] M.Q. Ou, X.C. Hao, B.F. Wan, T. Liang, Y.C. Ma, K. Liu, J. Mater. Sci. Technol. **33**, 1300 (2017)
[9] X.C. Hao, L. Zhang, X. Zhao, T. Liang, Y.C. Ma, K. Liu, Mater. Sci. Forum **816**, 586 (2015)
[10] M.Q. Ou, Y.C. Ma, H.L. Ge, B. Chen, S.J. Zheng, K. Liu, Mater. Sci. Eng. A **736**, 76 (2018)
[11] W.Z. Wang, T. Jin, J.L. Liu, Mater. Sci. Eng. A **479**, 148 (2008)
[12] M. Nathal, L. Ebert, Metall. Mater. Trans. A **16**, 1863 (1985)
[13] Q.Y. Shi, X.F. Ding, M.L. Wang, Metall. Mater. Trans. A **45**, 1833 (2014)
[14] G.L. Chen, L.Z. Zhuang, J.L. Xu, Acta Metall. Sin. **22**, 453 (1987). **(in Chinese)**
[15] S. Ma, L. Carrol, T.M. Pollock, Acta Mater. **55**, 5802 (2007)
[16] C.Y. Cui, Y.F. Gu, Y. Yuan, H. Harada, Scr. Mater. **64**, 502 (2011)
[17] F. Xue, H.J. Zhou, Q. Feng, MATEC Web Conf. **14**, 15002 (2014)
[18] C.M.F. Rae, R.C. Reed, Acta Mater. **49**, 4113 (2001)
[19] G. Lvov, V.I. Levit, M.J. Kaufman, Metall. Mater. Trans. A **35**, 1669 (2004)
[20] W. Sun, X.Z. Qin, J.T. Guo, L.H. Lou, L.Z. Zhou, Acta Metall. Sin. **52**, 455 (2016). **(in Chinese)**
[21] J.X. Yang, Q. Zheng, X.F. Sun, H.R. Guan, Z.Q. Hu, Mater. Sci. **41**, 6476 (2006)
[22] J.X. Yang, Q. Zheng, X.F. Sun, H.R. Guan, Z.Q. Hu, Mater. Sci. Eng. A **429**, 341 (2006)
[23] S.M. Seo, I.S. Kim, J.H. Lee, C.Y. Jo, H. Miyahara, K. Ogi, Metall. Mater. Trans. A **38**, 883 (2007)
[24] J. Wang, Master thesis, Institute of Metal Research, Chinese Academy of Sciences, Shenyang, 2011 (**in Chinese**)
[25] Y.L. Xu, L. Zhang, J. Li, X.S. Xiao, X.L. Cao, G.Q. Jia, Z. Shen, Mater. Sci. Eng. A **544**, 48 (2012)
[26] G.N. Maniar, J.E. Bridge, Metall. Trans. **2**, 95 (1971)
[27] G.N. Maniar, J.E. Bridge, H.M. James, Metall. Trans. **2**, 1484 (1971)
[28] J.X. Zhang, J.C. Wang, H. Harada, Y. Koizumi, Acta Mater. **53**, 4623 (2005)
[29] T. Link, A. Epishin, B. Fedelich, Philos. Mag. **89**, 1141 (2009)
[30] X.M. Dong, X.L. Zhang, K. Du, Y.Z. Zhou, T. Jin, H.Q. Ye, J. Mater. Sci. Technol. **28**, 1031 (2012)
[31] X.Z. Qin, J.T. Guo, C. Yuan, C.L. Chen, J.S. Hou, H.Q. Ye, Mater. Sci. Eng. A **485**, 74 (2008)
[32] M.E. Kassner, T.A. Hayes, Int. J. Plast. **19**, 1715 (2003)
[33] T. Krol, D. Baither, E. Nembach, Acta Mater. **52**, 2095 (2004)
[34] C.N. Wei, H.Y. Bor, L. Chang, J. Alloys Compd. **509**, 5708 (2011)
[35] Y.S. Lim, D.J. Kim, S.S. Hwang, H.P. Kim, S.W. Kim, Mater. Charact. **96**, 28 (2014)
[36] M.Q. Ou, X.C. Hao, Y.C. Ma, R.C. Liu, L. Zhang, K. Liu, J. Alloys Compd. **732**, 107 (2018)